

Third density and acoustic virial coefficients of helium isotopologues from ab initio calculations

Daniele Binosi,^{1, a)} Giovanni Garberoglio,^{1, b)} and Allan H. Harvey^{2, c)}

¹⁾European Centre for Theoretical Studies in Nuclear Physics and Related Areas (FBK-ECT*), Trento, I-38123, Italy.

²⁾Applied Chemicals and Materials Division, National Institute of Standards and Technology, Boulder, CO 80305, USA.

(Dated: 7 May 2024)

Improved two-body and three-body potentials for helium have been used to calculate from first principles the third density and acoustic virial coefficients for both ^4He and ^3He . For the third density virial coefficient $C(T)$, uncertainties have been reduced by a factor of 4–5 compared to the previous state of the art; the accuracy of first-principles $C(T)$ now exceeds that of the best experiments by more than two orders of magnitude. The range of calculations has been extended to temperatures as low as 0.5 K. For the third acoustic virial coefficient $\gamma_a(T)$, we applied the Schlessinger Point Method, which can calculate γ_a and its uncertainty based on the $C(T)$ data, overcoming some limitations of direct path-integral calculation. The resulting γ_a are calculated at temperatures down to 0.5 K; they are consistent with available experimental data but have much smaller uncertainties. The first-principles data presented here will enable improvement of primary temperature and pressure metrology based on gas properties.

CONTENTS

I. Introduction	1	1. The second acoustic virial coefficient for ^4He	18
II. Ab-initio calculation of virial coefficients	2	2. The third acoustic virial coefficient for ^4He	18
A. Uncertainty budget	2	Acknowledgments	15
B. The third density virial coefficient	4	I. INTRODUCTION	
C. The third acoustic virial coefficient	4		
III. Statistical Schlessinger Point Method	5		
A. Description of the method	5		
B. The second acoustic virial coefficient	6		
IV. Results and discussion	8		
A. Helium-4	8		
1. Third virial coefficient, $C(T)$	8		
2. Third acoustic virial coefficient, $RT\gamma_a$	10		
3. Comparison with experiment	11		
B. Helium-3	12		
1. Third virial coefficient, $C(T)$	12		
2. Third acoustic virial coefficient, $RT\gamma_a$	13		
V. Conclusions	13		
A. Small variance estimation of acoustic virial coefficients	16		
1. Second acoustic virial	16		
2. Third acoustic virial	17		
a. The two-body contribution	17		
b. The three-body contribution	17		
B. Statistical Schlessinger Point Method	18		

In recent years, great advances in gas-based pressure and temperature metrology have been enabled by the ability to calculate properties of small numbers of helium atoms from first principles with much smaller uncertainties than they can be measured. When combined with the ability to make highly precise electromagnetic or acoustic measurements on gas samples, the absolute temperature or the thermodynamic pressure can now be measured with smaller uncertainties than previously possible. The primary methods for state-of-the-art temperature metrology are acoustic gas thermometry,¹ dielectric-constant gas thermometry,² and refractive-index gas thermometry.^{3,4} We also note the recent development of a primary pressure standard based on dielectric measurements of helium.^{5,6} A recent review describes the contributions of first-principles calculated gas properties for precision temperature and pressure metrology.⁷

A key component of these efforts is the calculation of the virial coefficients that describe the deviation from ideal-gas behavior. For a gas of molar density ρ at temperature T , the virial expansion is

$$\frac{p}{\rho RT} = 1 + B(T)\rho + C(T)\rho^2 + \dots, \quad (1)$$

where p is the pressure and R is the molar gas constant. The second virial coefficient $B(T)$ depends on the interaction between two molecules, the third virial coefficient $C(T)$ depends on interactions among three molecules, and so on.

^{a)}Electronic mail: binosi@ectstar.eu

^{b)}Electronic mail: garberoglio@ectstar.eu

^{c)}Electronic mail: allan.harvey@nist.gov

The state-of-the-art pair potential for helium incorporates higher-order effects (adiabatic correction to the Born–Oppenheimer approximation, relativistic effects, quantum electrodynamics) to produce extremely small uncertainties in the potential over the entire physically relevant range of distances.⁸ It has been used to calculate values of $B(T)$ over a wide temperature range; this calculation benefits from the fact that an exact quantum calculation of $B(T)$ can be performed with a phase-shift method. The relative uncertainty of $B(T)$ for ^4He near room temperature is now on the order of 10^{-5} , and the uncertainties for ^3He are similar.⁸

For the third virial coefficient $C(T)$, no exact quantum solution is known, but the path-integral Monte Carlo (PIMC) method can be used to incorporate quantum effects with an accuracy limited only by the available computing resources. The last comprehensive first-principles calculations of $C(T)$ were published by Garberoglio *et al.* in 2011.^{9,10} These calculations used the pair potential of Cencek *et al.*,¹¹ which has been superseded by the 2020 work of Czachorowski *et al.*⁸ that yields uncertainties in B smaller by a factor of 5–10. It also used the three-body potential reported by Cencek *et al.*,¹² which has recently been improved upon by the work of Lang *et al.*¹³

At low temperatures, the uncertainty of the 2011 values of $C(T)$ was dominated by the convergence of the PIMC calculations; limitations on computing resources resulted in a lower limit of 2.6 K for the calculated results. At higher temperatures, the largest contribution to the uncertainty of $C(T)$ was that due to the uncertainty of the three-body potential.

We are now in a position to improve on the 2011 calculations in several ways. The uncertainty due to the potentials will be greatly reduced by using state-of-the-art two-body⁸ and three-body¹³ potentials; the new potentials reduce that component of our uncertainty by approximately a factor of 5 throughout the entire temperature range. We are able to reduce the statistical uncertainty from the PIMC calculation not only through increased computing power, but also by an improved propagator that accelerates the PIMC convergence. This allows us to compute values of $C(T)$ down to 0.5 K, with the statistical uncertainty only becoming the dominant uncertainty contribution below 2 K. We have also developed a more rigorous method for estimating the component of the uncertainty in $C(T)$ that results from uncertainties in the potentials used.

A related quantity of interest is the third acoustic virial coefficient γ_a , which arises in a low-density expansion [similar to Eq. (1)] for the sound speed around its ideal-gas value and is essential for acoustic gas thermometry. In the 2011 work,¹⁰ slow convergence of the PIMC calculations limited the accuracy attainable for γ_a . In this work, we introduce novel computational methods that enable a significant reduction of the uncertainty of the calculation of the acoustic virials. Nevertheless, our results are still limited by the statistical uncertainty of the Monte Carlo calculations for $T \leq 100$ K. We also present

a novel method of deriving $\gamma_a(T)$ from $C(T)$ data, and we argue that it provides an upper-bound estimate of the propagated uncertainty.

II. AB-INITIO CALCULATION OF VIRIAL COEFFICIENTS

The calculation of virial coefficients has been performed using the latest pair⁸ and three-body¹³ potentials for helium. These potentials come with well-defined uncertainty estimates, which we will assume to correspond to an expanded $k = 2$ uncertainty. We note that, due to the inclusion of relativistic effects, the pair potential for ^3He is slightly different from that for ^4He . In principle, a similar difference exists for the three-body potential, but this difference would be much smaller than the uncertainty in the potential so we use the three-body potential derived for ^4He in Ref. 13 for both isotopes.

In previous calculations, it was noted that the largest contribution to the uncertainty of the third virial coefficient was due to the propagated uncertainty of the three-body potential.^{10,14} The higher accuracy of the three-body potential used in this work, which resulted in uncertainties reduced by 3 to 5 times with respect to the previous potential,¹³ required us to develop some improved approaches for the calculation of the virial coefficients. Since the general framework is still the same as in our previous work,^{7,9,10} we will briefly describe the new methods developed for the present work.

A. Uncertainty budget

Before presenting the main results of this paper, it is worth examining the various contribution to the uncertainty budget of our calculations. In general, there are three sources: the statistical uncertainty of the path-integral Monte Carlo calculations, and the propagated uncertainties from the pair and three-body potentials. The latter two contributions can be further separated into contributions from Boltzmann statistics (indistinguishable particles, which is the leading contribution to $C(T)$ at $T > 4$ K), and from the odd and even exchanges, which depend on the bosonic or fermionic nature of the isotope under consideration and become relevant at low temperatures.

In our earlier works, we used two methods to propagate the uncertainty from the potentials to the third virial coefficient. In the first,^{9,10,14} we would compute the virial coefficients with modified potentials (adding and subtracting their uncertainty) and compute the uncertainty from the difference between these values. This approach is reasonably good at high temperatures, but fails at the lowest ones because the statistical uncertainty of the Monte Carlo calculation becomes large, and one needs to perform very computationally intensive calculations to reduce it significantly. Additionally, a rigid shift

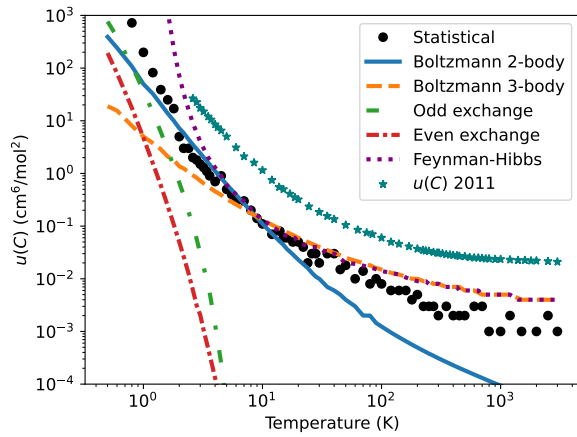


FIG. 1. Uncertainty budget for $C(T)$ of ${}^4\text{He}$ in the present work.

of the pair potential in the case of virial coefficients higher than the second may result in a positive, negative, or zero shift in the virial coefficient, thus calling into question on the validity of this approach.

Recently, we developed an alternative method that evaluates the propagated uncertainty by performing functional differentiation of the formula for $C(T)$ with respect to the potentials.¹⁵ We used a semiclassical approach using the fourth-order Feynman–Hibbs effective potential to evaluate the propagated uncertainty, which we deemed adequate for the scope of our previous calculations.

In this work, we extend this latter method by taking the functional derivative directly on the path-integral expression for $C(T)$. Consequently, our expression for the propagated uncertainty from the potential is valid at all temperatures. It turns out that the computational effort to determine the propagated uncertainties using this approach is much smaller than that needed to compute virial coefficients. Hence, we could evaluate the uncertainty in $C(T)$ propagated from the potentials. Subsequently, we conducted extensive Monte Carlo simulations aimed at reducing the statistical error to a level below the uncertainty attributed to the potentials.

An overview of the uncertainty budget in the case of ${}^4\text{He}$ is shown in Fig. 1. The situation for ${}^3\text{He}$ is very similar and is not reported here.

First of all, we can retrospectively gauge the validity of the Feynman–Hibbs fourth-order semiclassical estimation of the propagated uncertainty using the functional differentiation approach. Inspection of Fig. 1 shows that this approximation is quite good for $T \geq 4$ K. At lower temperatures, the uncertainty obtained with the semiclassical approach generally exceeds that obtained using the rigorous path-integral estimation and tends to increase quite rapidly.

We also compare the uncertainty with the new potentials to the uncertainty of our previous calculation, reported with starred symbols.¹⁰ As already pointed out

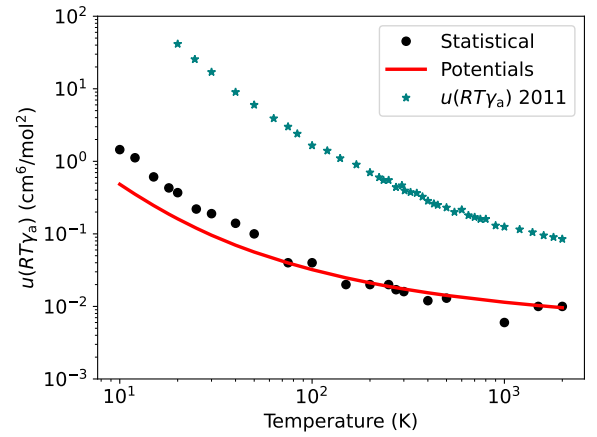


FIG. 2. Uncertainty budget for $RT\gamma_a(T)$ of ${}^4\text{He}$ in the present work.

in Ref. 13, the accuracy of the new potentials, especially the three-body surface, results in a reduction of the uncertainty by roughly a factor of 5 (and sometimes more) at all temperatures above 2.6 K.

Additionally, the increased accuracy of the potential energy surfaces required us to develop improved calculation methods, in order to be able to reduce the statistical Monte Carlo uncertainty below that propagated from the potentials. As will be described below, we used enhanced propagators in the calculation of $C(T)$ and a novel approach based on the idea of the *virial* estimator of the kinetic energy in path-integral Monte Carlo calculations to reduce the uncertainty of $RT\gamma_a$.

In the case of $C(T)$, this approach was successful for $T \geq 2$ K, where the uncertainty budget is dominated by the uncertainty propagated from the potentials. At lower temperatures, the uncertainty budget is dominated by the Monte Carlo contribution.

The uncertainty budget for the third acoustic virial coefficient, $RT\gamma_a$, is reported in Fig. 2. Also in this case, the propagation of the uncertainty from the pair and three-body potentials has been performed by functional differentiation of the path-integral expression for $RT\gamma_a$, which is reported in the Supplementary Material. Compared with our previous results,¹⁰ we can see that the combination of more accurate potentials and reduced-variance estimators resulted in a reduction of the uncertainty by more than one order of magnitude. However, despite our computational efforts, the statistical uncertainty still dominates the budget at temperatures $T \leq 100$ K, up to a factor between 2 and 3. In order to overcome this limitation in the direct calculation of $RT\gamma_a$, we used the statistical Schlessinger Point Method (SPM) to derive the third acoustic virial and its uncertainty directly from the results for $C(T)$. This approach, as we will detail below, provides us with the most accurate estimation of $RT\gamma_a$ and its uncertainty at low temperatures.

B. The third density virial coefficient

The virial expansion of Eq. (1) is a rigorous result of quantum statistical mechanics, which also provides an exact formula relating $C(T)$ and the interaction among three particles. $C(T)$ is conveniently evaluated using the path-integral formulation of quantum statistical mechanics that enables rewriting the expression for $C(T)$ involving three quantum particles into an equivalent classical expression involving three ring polymers of P beads each; the correspondence is exact in the $P \rightarrow \infty$ limit.^{9,16}

This equivalence is based on the Trotter–Suzuki identity, which – in the case of a quantum Hamiltonian $H = T + V$, where T is the kinetic energy and V is the potential energy – is written as

$$e^{-\beta(T+V)} = \lim_{P \rightarrow \infty} \left(e^{-\beta T/P} e^{-\beta V/P} \right)^P. \quad (2)$$

In actual calculations, one uses a finite value of P , which has to be taken large enough so that the results obtained are converged to within a specified uncertainty. For the calculation of virial coefficients, it is found that the optimal value of P is inversely proportional to the temper-

ature and that $PT \sim 2400$ K for helium. The straightforward use of Eq. (2) implies that calculations at lower temperature become progressively more demanding.

One way to overcome this difficulty is to develop more accurate approximations of the right-hand side of Eq. (2). This idea was first put forward by Takahashi and Imada¹⁷ and subsequently developed by Kono *et al.*¹⁸ and by Li and Broughton.¹⁹ The latter authors showed that a more accurate and effective approximation of the Trotter–Suzuki expansion is

$$e^{-\beta(T+V)/P} \sim e^{-\beta T/P} e^{-\beta V/P} e^{-(\beta/P)^3 W/24} \quad (3)$$

$$W = [[V, T], V] = \frac{\hbar^2}{m} |\nabla V|^2. \quad (4)$$

In the case of three particles, the potential V can be expressed as a function of the distances between the pairs, that is r_{12} , r_{13} , and r_{23} , as

$$V = U_2(r_{12}) + U_2(r_{13}) + U_2(r_{23}) + U_3(r_{12}, r_{13}, r_{23}), \quad (5)$$

where $U_2(r)$ is the pair potential and $U_3(r_{12}, r_{13}, r_{23})$ is the non-additive part of the three-body potential. In this case, the squared gradient appearing in Eq. (4) can be written as

$$|\nabla V|^2 = 2 \left| \frac{\partial V}{\partial r_{12}} \right|^2 + 2 \left| \frac{\partial V}{\partial r_{13}} \right|^2 + 2 \left| \frac{\partial V}{\partial r_{23}} \right|^2 + \frac{\partial V}{\partial r_{12}} \frac{\partial V}{\partial r_{13}} \cos \theta_1 + \frac{\partial V}{\partial r_{12}} \frac{\partial V}{\partial r_{23}} \cos \theta_2 + \frac{\partial V}{\partial r_{13}} \frac{\partial V}{\partial r_{23}} \cos \theta_3, \quad (6)$$

where θ_i is the internal angle at particle i in the triangle made by the three particles.

In the actual calculations, it has been found convenient to compute $C(T)$ as the sum of two parts: the first is obtained considering pair potentials only (that is, assuming $U_3 = 0$), whereas the second part is the contribution due to the non-zero value of U_3 .^{15,20} In general, the most time-consuming part of the calculation involves the contribution from the pair potential, whereas the non-additive contribution to $C(T)$ is much less computationally demanding. Therefore, we have used the standard *primitive* approximation²¹ of Eq. (2) for the latter contribution, and the Li–Broughton approximation of Eq. (3) for the pair contribution only. In this latter case, we found that we could reach well-converged results using $P = \text{nint}(4 + \sqrt{120 \text{ K}/T})$ and $P = \text{nint}(4 + \sqrt{160 \text{ K}/T})$ for ^4He and ^3He , respectively. The function $\text{nint}(x)$ denotes the nearest integer to x . The values of P needed using the Li–Broughton approach should be compared with the values $P = \text{nint}(4 + 2400 \text{ K}/T)$ that are needed, irrespective of the isotope, to reach convergence using the primitive approximation, and that was used to compute the non-additive contribution to $C(T)$. In the case of the Li–Broughton approximation, a much smaller number of beads is needed to reach convergence in the path-integral results. This more than offsets the additional calculations

needed to evaluate the quantity W of Eq. (4).

At low temperatures, quantum statistical effects contribute to the value of the third virial coefficient. We evaluated these contributions using the primitive approximation, which is the same approach adopted in Ref. 9.

C. The third acoustic virial coefficient

The acoustic virial coefficients appear in the pressure expansion of the speed of sound u , according to

$$u^2 = \frac{\gamma_0 RT}{M} \left[1 + \beta_a \frac{p}{RT} + \gamma_a \frac{p^2}{RT} + \dots \right], \quad (7)$$

where $\gamma_0 = 5/3$ for a monoatomic gas and M is the molar mass. β_a and $RT\gamma_a$ can be calculated from the first and second temperature derivatives of the second and third

density virial coefficients according to the formulae²²

$$\beta_a(T) = \underbrace{2B}_1 + \underbrace{2(\gamma_0 - 1)T \frac{dB}{dT}}_2 + \underbrace{\frac{(\gamma_0 - 1)^2}{\gamma_0} T^2 \frac{d^2B}{dT^2}}_3, \quad (8)$$

$$Q = B + (2\gamma_0 - 1)T \frac{dB}{dT} + (\gamma_0 - 1)T^2 \frac{d^2B}{dT^2} \quad (9)$$

$$RT\gamma_a = \frac{\gamma_0 - 1}{\gamma_0} Q^2 - \beta_a(T)B(T) + \frac{2\gamma_0 + 1}{\gamma_0} C + \frac{\gamma_0^2 - 1}{\gamma_0} T \frac{dC}{dT} + \frac{(\gamma_0 - 1)^2}{2\gamma_0} T^2 \frac{d^2C}{dT^2}, \quad (10)$$

where we have indicated three terms (1, 2, and 3) in β_a for later convenience.

As noted in Ref. 10 the path-integral expression used for the calculation of $RT\gamma_a$ involves, due to the presence of temperature derivatives, expressions analogous in form to the so-called *thermodynamic* kinetic energy estimator, which is known to have a large variance.²³ As a consequence, in the calculations of $RT\gamma_a$ the largest part of the uncertainty was due to the statistical uncertainty of the Monte Carlo calculations.

In order to reduce this effect as much as possible, we developed a new approach based on the same ideas that led to the *virial* estimator of the kinetic energy.²⁴ The lengthy derivations of the path-integral formulae leading to a reduced-variance estimation of the third acoustic virial coefficient are reported in the Supplementary Material. However, as we discuss in the following, even these improved formulae, which resulted in a reduction of the statistical uncertainty in the path-integral Monte Carlo evaluation of $RT\gamma_a$ by more than one order of magnitude at $T = 20$ K, were not enough to reduce the statistical uncertainty below that propagated from the potentials at the lowest temperatures investigated in this work.

In order to provide more accurate estimates of the acoustic virial coefficients, we employ the Schlessinger Point Method (SPM). The SPM allows us to compute the first and second temperature derivatives, and their uncertainties, directly from our calculated $C(T)$ data, removing the need to simulate the acoustic virials.

III. STATISTICAL SCHLESSINGER POINT METHOD

A. Description of the method

Let us denote by D_N the set of all the N computed pairs of some virial coefficient v_i associated with a given temperature T_i :

$$D_N = \{(T_i, v_i = v(T_i)), i = 1, \dots, N\}. \quad (11)$$

Within a subset $D_M \subseteq D_N$ (with $M < N$), one can construct the Schlessinger Point Method (SPM) continued

fraction interpolator²⁵

$$I_M(T) = \frac{v_1}{a_1(T - T_1)}, \quad (12)$$

$$1 + \frac{a_2(T - T_2)}{1 + \frac{\dots}{1 + \frac{\dots}{1 + \frac{\dots}{a_{M-1}(T - T_{M-1})}}}}$$

where the $M - 1$ coefficients a_i are recursively determined from the formulas

$$(T_2 - T_1)a_1 = v_1/v_2 - 1, \quad (13a)$$

$$(T_\ell - T_{\ell+1})a_\ell = 1 + \frac{a_{\ell-1}(T_{\ell+1} - T_{\ell-1})}{1 + \frac{a_{\ell-2}(T_{\ell+1} - T_{\ell-2})}{1 + \frac{a_{\ell-3}(T_{\ell+1} - T_{\ell-3})}{\dots}}}, \quad (13b)$$

$$1 + \frac{a_1(T_{\ell+1} - T_1)}{1 - v_1/v_{\ell+1}}$$

and are such that $I_M(T_i) = T_i, \forall T_i \in D_M$.

The interpolator (12) can be cast in the rational form

$$I_M(T) = \frac{P_M(T)}{Q_M(T)}, \quad (14)$$

where P_M and Q_M are polynomials whose degree is determined by the size M of the subset D_M chosen: $(M - 1)/2$ (both P_M and Q_M) if M is odd; $M/2 - 1$ (P_M) and $M/2$ (Q_M) if M is even. Thus, for large T , $I_M \sim \text{const.}$ (respectively, $I_M \sim 1/T$) for M odd (respectively, even).

While the SPM shares the same rational expression of Eq. (14) with a Padé approximant, the idea behind it is completely different. The latter is in fact defined as an expansion of a function near a specific point: its coefficients are thus constructed from values of higher derivatives at that point, so that the approximant's power series agrees with that of the original function. In the case of SPM, Eq. (14) is rather constructed using the original function values at *different* points.²⁶ Thus, I_M is able to capture the behavior of v over a range of values extending beyond that of D_M (and even D_N) without the need to compute any derivatives.

How well the interpolator of Eq. (12) is capable of reproducing the entire dataset D_N – and, correspondingly, the function v – mainly depends on the precision of the starting dataset D_N . For example, when exact numerical data are considered as in Eq. (11), I_M is practically indistinguishable from v independent of the number M of points in D_M (provided that the latter is large enough to capture the basic features of the curve v we wish to describe). However, in the presence of uncertainties one has

$$D_N = \{(T_i, v_i, \epsilon_i), i = 1, \dots, N\}. \quad (15)$$

so that the v_i are statistically distributed around the true curve v with variance ϵ_i .

A veracious reconstruction of the function v can be obtained also in this case if the SPM is combined with resampling to propagate uncertainties. To this end, we generate from Eq. (15) a replica set D_N^r by randomly drawing from each v_i in D_N a new one v_i^r from a normal distribution \mathcal{N} with a mean value equal to v_i and a standard deviation equal to its associated standard uncertainty ϵ_i :

$$D_N^r = \{(T_i, v_i^r = \mathcal{N}(v_i, \epsilon_i)), i = 1, \dots, N\}. \quad (16)$$

Next, fixing M at a suitable value,²⁷ we randomly choose the subset $D_M^r \subseteq D_N^r$ and proceed to construct the corresponding SPM interpolator I_M^r from Eq. (12). Repeating these steps for a sufficiently large number of replicas n^r gives rise to a large population of interpolators that can be filtered according to suitable criteria.

More specifically, we require that the interpolator I_M^r is such that: *i*) it is smooth (continuous with all its derivatives, $I_M^r \in C^\infty$) on the positive real axis²⁸ $\mathbb{R}_{>0}$; *ii*) it deviates less than ϵ_i from 95% of the remaining $N - M$ points in D_N .

For the specific cases of the second and third virial coefficients studied here, these conditions are very stringent: using the data computed in Ref. 8 for B , only $\sim 0.002\%$ (^3He) and $\sim 0.01\%$ (^4He) of the constructed interpolators satisfied them; and those percentages drastically drop for C using the data computed in this paper (as in this case D_N contains fewer data with larger uncertainties), where one has a mere 0.0003% (further down to 0.00001%) in the ^3He (^4He) cases, respectively.

Each of the derived curves can be utilized to construct a smooth description of the second (β_a) and third ($RT\gamma_a$) acoustic virial coefficients by directly applying Equations (8) and (10). However, this process involves calculating up to second-order derivatives of the constructed interpolators, which may introduce spurious oscillations into the resulting curves. The curves displaying these fluctuations are removed from the final set of interpolators. Thus, one obtains a different number of interpolators for the B and C virial coefficients in the ^4He and ^3He cases. However, as both B and C enter in the calculation of $RT\gamma_a$ the minimum number of available interpolators between B and C is retained: more specifically, one ends up with 587 SPM interpolators for the ^4He B and C virial coefficients and 378 for the ^3He ones.

This continuous framework allows for the evaluation of virial coefficients at any specified temperature. Here, the SPM output represents the average of the interpolator curve values at the given temperature, with the uncertainty derived straightforwardly from the standard deviation of these values.

B. The second acoustic virial coefficient

To examine the capability of the SPM method in estimating uncertainty propagation for acoustic virials, we investigated in detail its performance in the case of the

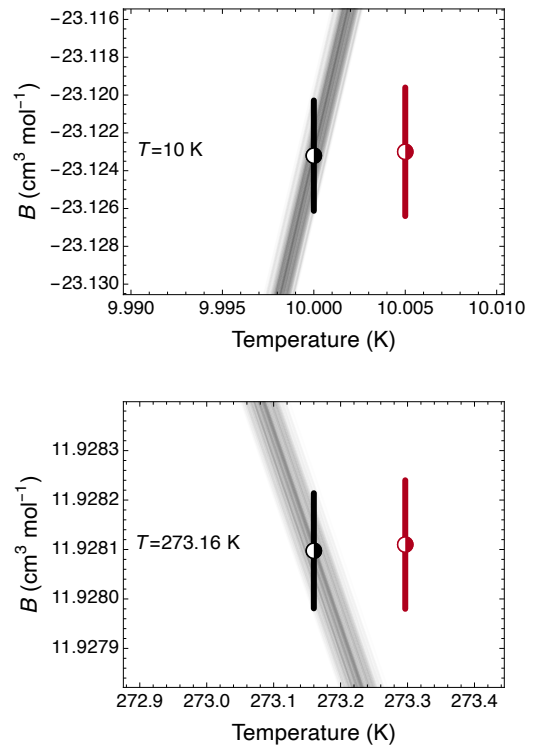


FIG. 3. Interpolating curves generated using the SPM method in the case of $B(T)$ for ^4He at $T = 10$ K (upper panel) and $T = 273.16$ K (lower panel). The black symbol denotes the average value and $k = 2$ expanded uncertainty derived from the SPM curves. The red symbol, which has been displaced to the right for the sake of clarity, reports the average value and expanded uncertainty from the original calculation.⁸

second acoustic virial coefficient $\beta_a(T)$ of ^4He from $B(T)$ data, comparing it with the direct calculation using the phase-shift method.⁸

We first present in Fig. 3 the SPM interpolators that reproduce $B(T)$ and its uncertainty at two temperatures (additional illustrative plots are available in the Supplementary Material). One can see that the set of SPM curves reproduces quite well the average value and expanded uncertainty of $B(T)$ across a wide temperature range.

The second acoustic virial coefficient $\beta_a(T)$ of ^4He computed with SPM is shown in Fig. 4, where we also compare it with the direct calculations, at the same two temperatures as in Fig. 3 (also in this case, the plots for more temperatures are shown in the Supplementary Material). We see that the SPM-derived values are in very good agreement with the ones obtained by direct computation,⁸ however, in this case the SPM approach provides an uncertainty higher than that computed as the difference of the values of $\beta_a(T)$ obtained with rigidly shifted potentials.

We show in Fig. 5 the ratio between the SPM estimated uncertainty of $\beta_a(T)$ and the uncertainty computed in

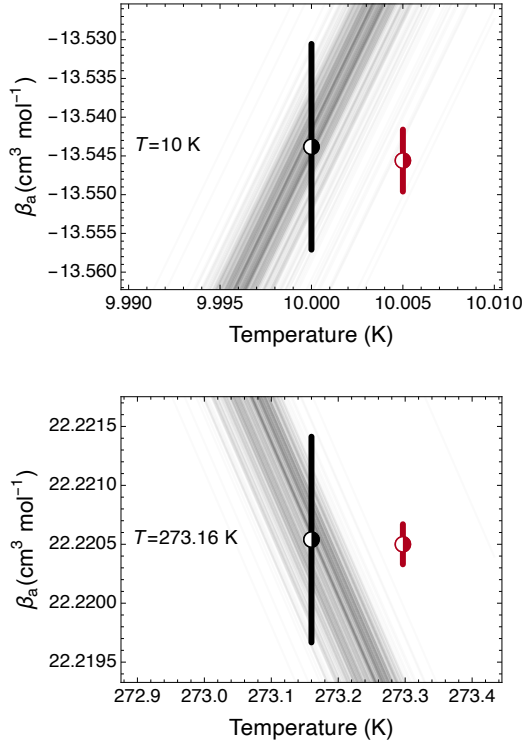


FIG. 4. Interpolating curves generated using the SPM method in the case of $\beta_a(T)$ for ${}^4\text{He}$ at $T = 10$ K (upper panel) and $T = 273.16$ K (lower panel). The black symbol denotes the average value and $k = 2$ expanded uncertainty derived from the SPM curves. The red symbol, which has been displaced to the right for the sake of clarity, reports the average value and expanded uncertainty from the original calculation.⁸

Ref. 8. We notice that SPM tends to significantly overestimate the uncertainty at the boundaries of the temperature range considered. SPM estimates close to the boundaries could be improved by adding knowledge of the limiting behavior of $B(T)$ (*e.g.*, a known power-law dependence on T), but we did not pursue this further in this paper, because uncertainty propagation using PIMC methods can be performed efficiently even with limited computational resources at high temperature, and there is presently no theoretical treatment of exchange effects for acoustic virial coefficients, which are expected to contribute significantly below ≈ 5 K. Due to the aforementioned SPM behavior at the boundaries of the temperature range, we will report $RT\gamma_a$ and its uncertainty evaluated with SPM down to $T = 1$ K (see Supplementary Material).

In the intermediate temperature region, however, the SPM uncertainty estimates of β_a are 3 to 4 times larger than those computed in Ref. 8. The main reason for this result is that the SPM method is statistical in nature, and it is based on generating a series of smooth curves that interpolate $B(T)$ values and their estimated uncertainty. For each of these curves, one calculates the

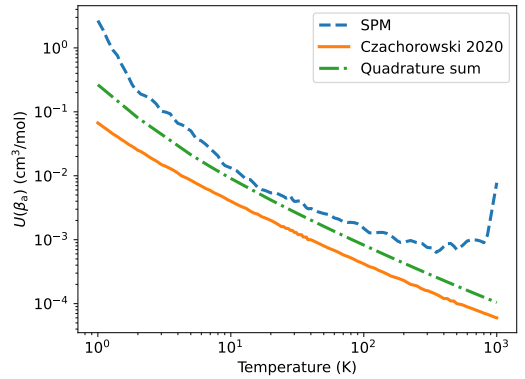


FIG. 5. Expanded ($k = 2$) uncertainty of $\beta_a(T)$ for ${}^4\text{He}$ as a function of temperature. Solid line: estimate from Ref. 8, obtained by the difference between the values of β_a computed using rigidly shifted potentials. Dashed line: estimate from the SPM approach. Dot-dashed line: sum in quadrature of the uncertainty propagated from the three terms 1, 2, and 3 in Eq. (8) using the functional differentiation approach.

temperature derivatives and evaluates $\beta_a(T)$ according to Eq. (8). The uncertainty of β_a is evaluated from the standard deviation of the distribution of the values of β_a at each temperature.

However, inspection of Eq. (8) for the acoustic virial shows that it is obtained as the sum of three terms (1, 2, and 3), each of which depends on the pair potential. When considering the effect of the uncertainty of the pair potential on $\beta_a(T)$, these three terms will most likely exhibit a correlated variation, which leads to cancellations since the contributions have opposite signs due to the shape of the $B(T)$ function. This correlated behavior is not taken into account by the SPM approach, which in fact provides a rigorous upper bound to the actual propagated uncertainty.

Another way to arrive at a similar conclusion is to consider the three terms delineated in Eq. (8). The approach used to propagate the uncertainty in Ref. 8 estimates it from

$$U(\beta_a) = \frac{1}{2} |\beta_a(T; u_2 + \delta u_2) - \beta_a(T; u_2 - \delta u_2)|, \quad (17)$$

where $\beta_a(T; u)$ denotes the value of the second acoustic virial coefficient computed using the pair potential u . This way of estimating uncertainty is based on a rigid shift of the pair potential u_2 according to its estimated uncertainty δu_2 and it is not statistical in nature. Notice also that it would include any correlation between the shifts of the three terms in Eq. (8) induced by a variation of δu_2 .

The effect of these correlations can be evaluated by computing the uncertainty of each of the three terms in Eq. (8) using the functional derivative method and adding them in quadrature. This procedure is tantamount to neglecting that all the terms would be indeed be affected by the *same* variation δu_2 of the underlying

pair potential, and in fact it produces propagated uncertainties that are approximately *twice* as much as those estimated in Ref. 8. The results of these calculations are reported as a dot-dashed line in Fig. 5.

From these considerations, we deduce that the SPM approach is a convenient way to propagate uncertainties, and that it leads to an *upper bound* of the actual uncertainty that would be obtained by either a rigid shift of the potential or, in the case of higher-order coefficients, by the functional differentiation approach.^{7,15}

IV. RESULTS AND DISCUSSION

A. Helium-4

1. Third virial coefficient, $C(T)$

The values of $C(T)$ for ^4He are reported in Tables I and II. At low temperatures, where quantum exchange effects are significant, $C(T)$ is obtained as a sum of three terms:⁹ the first corresponds to Boltzmann statistics (distinguishable particles), and is the only term that contributes at high temperatures, whereas the other two terms come from the odd and even exchange terms in the partition function. Analogously to our previous findings, exchange effects are appreciable only for temperatures $T \leq 6$ K.

Please note that we have slightly changed our notation for the exchange contribution compared to Ref. 9. The definition of the Boltzmann component remained the same, whereas contributions from the old quantity C_B have been included in the new definition of C_{odd} and C_{even} which now include *all* the terms that involve an odd or even permutation, respectively.¹⁵ This change corresponds to how the various contributions are calculated: we found it convenient to collect all similar terms in the same calculation in order to reduce the statistical variance. Additionally, the odd and even contributions already contain the weights coming from considering the nuclear spin I , so that we have $C(T) = C_{\text{Boltz}} + C_{\text{odd}} + C_{\text{even}}$ irrespective of the isotope.

In order to facilitate comparisons with other results in the literature, we developed a correlation for the values of a generic virial coefficient $F(T)$ and its expanded uncertainty $U(F)$ in the form of

$$F(T) = \sum_{k=1}^n \frac{a_k}{(T/T_0)^{b_k}}, \quad (18)$$

$$U(F) = a \exp\left(\frac{b}{(T/T_0)^c}\right), \quad (19)$$

which smoothly interpolates the Monte Carlo data for $F = C$, passing within the expanded ($k = 2$) uncertainty $U(F)$ at all the temperatures in the range $2 \text{ K} \leq T \leq 3000 \text{ K}$. The limitation in the temperature range of the correlation is because the rapid decrease of $C(T)$ below $T = 2 \text{ K}$ prevented us from finding a satisfactory set of parameters for Eq. (18). The parameters of Eq. (18) for

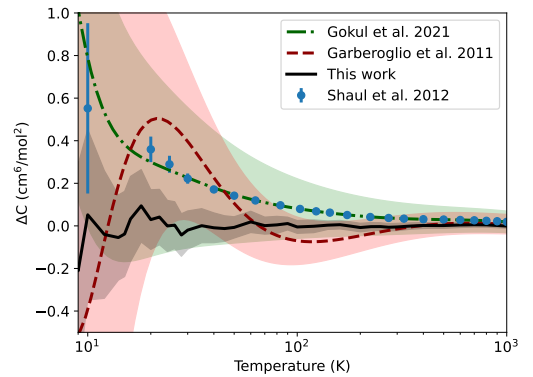


FIG. 6. Comparison of literature results for $C(T)$ in the case of ^4He . We use as a baseline the correlation of Eq. (18). The black line and gray shading show the results and the expanded ($k = 2$) uncertainty of the present calculations. The red area covers the results of our previous calculation in 2011.¹⁰ The dashed green line and the green area reports the results from the correlation developed by Gokul *et al.*²⁹ The blue dots are the results by Shaul *et al.*²⁰ In this latter case, the uncertainty is the expanded uncertainty of the Monte Carlo calculation.

helium isotopologues are given in Table III, while those for Eq. (19) are given in Table IV. We also report in Table III fitting parameters, assuming the same form as Eq. (18), obtained for $F = B$ using the data computed in Ref. 8. The correlations for $B(T)$ and $C(T)$ enable the calculation of $RT\gamma_a$ (see Eqs. (8)–(10)), and we have used these values as a cross check of the values obtained using the PIMC and SPM approaches.

The updated values of $C(T)$ computed in this work are compared with other literature results in Fig. 6. In general, the values obtained in the present work are compatible, within mutual uncertainties, with the other calculations. However, due to the use of updated two- and three-body potentials, the uncertainty is much smaller. Compared with the values of $C(T)$ obtained by the Kofke group,^{20,29} the present data show a downward shift. This is consistent with the finding that, due to relativistic effects, the new three-body potential is generally more attractive than the non-relativistic one used in all previous calculations.¹³

When compared to our previous results,¹⁰ this rigid shift is not apparent, although the two sets of values are mutually compatible. This might indicate incomplete convergence of some parameters (cutoff, number of beads) in our previous calculation.

In the case of the lowest temperatures, where exchange effects are significant, our new values are in very good agreement with results reported earlier.^{9,10} The data, shown in Fig. 7, agree within mutual uncertainties in the whole temperature range where the calculations overlap. In this case, the expected downward shift of $C(T)$ due to the more attractive three-body potential¹³ is much more evident that at the highest temperatures. This figure also shows the reduction in the uncertainty due to the

TABLE I. The third virial coefficient $C(T)$ and its expanded ($k = 2$) uncertainty $U(C)$ for ${}^4\text{He}$ at low temperatures. The other columns report the contributions due to Boltzmann statistics (C_{Boltz}), and the odd (C_{odd}) and even exchange (C_{even}), together with their standard ($k = 1$) statistical uncertainties due to the Monte Carlo calculation. The last column reports the combined standard ($k = 1$) uncertainty propagated from the pair and three-body potentials. Temperatures are in units of K and $C(T)$ in units of cm^6/mol^2 .

T	C	$U(C)$	C_{Boltz}	$u(C_{\text{Boltz}})$	C_{odd}	$u(C_{\text{odd}})$	C_{even}	$u(C_{\text{even}})$	$u(C_{\text{even}})$	u_{pot}
0.5	-2112555	20631	-779262	5189	-599309	4837	-733983	7437	882	
0.6	-962869	6194	-395907	1497	-246498	1816	-320464	1959	466	
0.8	-273391	1476	-136279	376	-50458	395	-86654	473	155	
1	-99878	418	-59453	129	-11042	115	-29383	99	63	
1.2	-42799	179	-29293	65	-1949	42	-11557	25	36	
1.4	-20359	88	-15533	32	150	19	-4976	10	22	
1.6	-10300	58	-8540	23	525	9	-2285	5	14	
1.8	-5308	39	-4685	14	479	10	-1102	2	10	
2	-2675	17	-2463	3	346	3	-557.0	1.6	7	
2.1768	-1298	14	-1238	3	250	2	-310.6	1.2	6	
2.4	-277	11	-281.5	1.9	160	2	-155.3	0.5	5	
2.6	272	9	247.7	1.7	108.7	1.4	-84.6	0.3	4	
2.8	612	7	584.9	1.3	74.6	1.2	-47.70	0.19	3	
3	817	6	796.3	1.2	48.1	0.9	-27.43	0.12	3	
3.2	943	5	926.2	1.1	33.2	0.6	-16.03	0.08	2	
3.4	1020	4	1007.3	1.0	22.7	0.5	-9.50	0.05	1.8	
3.6	1059	4	1048.9	0.8	15.4	0.5	-5.68	0.04	1.6	
4	1078	3	1072.9	0.7	7.3	0.3	-2.139	0.016	1.2	
4.222	1068	3	1064.7	0.9	4.9	0.1	-1.275	0.009	1.1	
4.5	1042	2	1040.2	0.5	2.9	0.2	-0.683	0.006	0.9	
5	983.8	1.6	982.7	0.4	1.35	0.11	-0.222	0.003	0.7	
5.5	919.5	1.3	919.1	0.3	0.48	0.05	-0.076	0.001	0.6	
6	856.8	1.1	856.6	0.3	0.21	0.03	-0.029	0.001	0.5	

TABLE II. The third virial coefficient $C(T)$ and its expanded ($k = 2$) uncertainty $U(C)$ for ${}^4\text{He}$. The last two columns reports the standard ($k = 1$) statistical uncertainty due to the Monte Carlo calculation and the combined standard ($k = 1$) uncertainty propagated from the pair and three-body potentials. Temperatures are in units of K and $C(T)$ in units of cm^6/mol^2 .

T	C	$U(C)$	$u(C_{\text{Boltz}})$	u_{pot}
7	745.5	0.8	0.2	0.3
8	656.5	0.6	0.14	0.3
9	586.1	0.5	0.11	0.2
10	530.6	0.4	0.07	0.17
12	449.5	0.3	0.08	0.13
13.8031	399.4	0.2	0.06	0.10
14	394.9	0.2	0.06	0.10
15	374.1	0.2	0.05	0.09
16	356.5	0.2	0.05	0.09
18	328.33	0.17	0.04	0.07
20	306.84	0.14	0.02	0.06
22	290.11	0.13	0.03	0.06
24	276.65	0.12	0.03	0.05
24.5561	273.42	0.11	0.02	0.05
26	265.66	0.11	0.03	0.05
28	256.43	0.10	0.03	0.04
30	248.65	0.09	0.015	0.04
35	233.38	0.08	0.018	0.04
40	222.00	0.07	0.010	0.03
45	213.04	0.06	0.014	0.03
50	205.68	0.05	0.008	0.03
54.3584	200.17	0.05	0.010	0.02
60	194.00	0.05	0.008	0.02
70	184.79	0.04	0.006	0.02
80	177.17	0.04	0.006	0.018
83.8058	174.57	0.04	0.006	0.017
90	170.63	0.03	0.004	0.016
100	164.86	0.03	0.005	0.015
120	155.07	0.03	0.003	0.013
140	146.92	0.02	0.003	0.012
160	139.94	0.02	0.003	0.011
180	133.84	0.02	0.002	0.010
200	128.44	0.02	0.003	0.010
225	122.487	0.019	0.002	0.009
234.3156	120.456	0.018	0.002	0.009
250	117.231	0.018	0.002	0.009
273.16	112.867	0.017	0.003	0.008
300	108.320	0.017	0.003	0.008
302.9146	107.860	0.016	0.001	0.008
325	104.495	0.018	0.004	0.008
350	101.003	0.015	0.001	0.007
375	97.796	0.016	0.003	0.007
400	94.840	0.014	0.002	0.007
429.7485	91.602	0.013	0.0011	0.007
450	89.550	0.013	0.0014	0.007
500	84.944	0.013	0.0018	0.006
600	77.274	0.012	0.0013	0.006
700	71.097	0.011	0.0010	0.005
800	65.983	0.011	0.0011	0.005
1000	57.939	0.010	0.0012	0.005
1200	51.848	0.009	0.0007	0.005
1500	44.974	0.009	0.0007	0.004
2000	37.043	0.008	0.0007	0.004
2500	31.596	0.008	0.0006	0.004
3000	27.579	0.008	0.0009	0.004

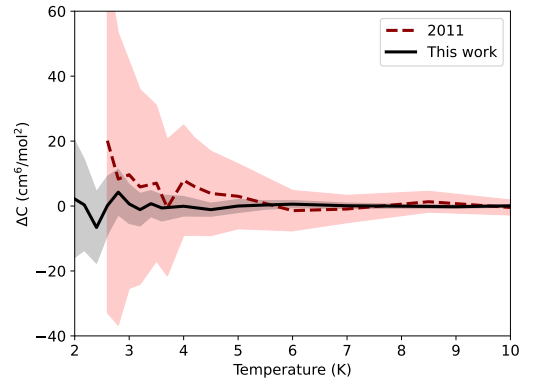


FIG. 7. Comparison with our previous results for $C(T)$ at low temperatures for ${}^4\text{He}$. We use as a baseline the correlation of Eq. (18). The black line and gray shading show the results and the expanded ($k = 2$) uncertainty of the present calculations. The results of our previous calculation in 2011^{9,10} are shown as a dashed red curve with light red shading for the expanded uncertainty.

much more accurate pair and three-body potentials used in this work.

2. Third acoustic virial coefficient, $RT\gamma_a$

Our results for the third acoustic virial coefficient for ${}^4\text{He}$ are reported in Table V and illustrated in Fig. 8. The values that we obtain are generally compatible with those calculated by Gokul *et al.*,²⁹ although also in this case a systematic downward shift – which we ascribe to the improved three-body potential – is more evident.

Figure 8 also reports the results of the SPM approach, obtained from the path-integral values of $C(T)$ computed in this work and the $B(T)$ values of Ref. 8. As mentioned above, computer time limitations prevented us from reducing the statistical uncertainty of $RT\gamma_a$ to a value comparable to the propagated uncertainty from the potential, in contrast to what we were able to do in the case of $C(T)$, at temperatures $T \leq 75$ K. At higher temperatures, the path-integral results are in very good agreement with those obtained by the SPM approach, although we notice that the SPM uncertainty is larger than the path-integral one for $T > 500$ K. In the low-temperature regime, the path-integral results follow closely the SPM values, whose uncertainty is, however, smaller. We did not develop our calculation methods for $RT\gamma_a$ to include exchange effects; hence the SPM approach is presently the only way to compute the third acoustic virial coefficient of helium isotopologues below ≈ 10 K and we suggest its use for $1 \text{ K} \leq T \leq 75 \text{ K}$. A table of SPM values for ${}^4\text{He}$ in the temperature range 1 – 1000 K is provided as Supplementary Material.

TABLE III. Parameters of the correlation in the right-hand side of Eq. (18) for the second and third virial coefficient of ^4He and ^3He . For both isotopes, the correlations have been fitted with data in the range 2 – 3000 K and are therefore not reliable outside this range. T_0 is given in K, the parameters b_i are dimensionless, and the parameters a_i have units of cm^3/mol for B and cm^6/mol^2 for C .

Parameter	$B(^4\text{He})$	$C(^4\text{He})$	$B(^3\text{He})$	$C(^3\text{He})$
n	6	8	6	6
T_0	100	100	100	100
a_1	-2.313629×10^{-7}	-8.677343×10^{-9}	$-4.753277 \times 10^{-10}$	-7.844580×10^{-4}
a_2	-2.600944×10^{-1}	-1.772954×10^1	1.976692×10^{-8}	-3.968348×10^2
a_3	-5.991829	1.501863×10^2	-1.743840×10^{-1}	1.242512×10^3
a_4	-3.191519×10^2	-5.865689×10^2	-1.431270×10^1	-2.009221×10^3
a_5	6.694613×10^2	1.086422×10^3	6.478292×10^1	2.054704×10^3
a_6	-3.323825×10^2	-1.671338×10^3	-3.825692×10^1	-7.205123×10^2
a_7	—	1.863898×10^3	—	—
a_8	—	-6.600046×10^2	—	—
b_1	4.327481	6.538462	6	3.740741
b_2	1.406369	2.142857	5.162791	1.272720
b_3	0.801565	1.823529	1.363636	1.142857
b_4	0.301418	1.526316	0.641026	0.9
b_5	0.260488	1.277778	0.2	0.64
b_6	0.225976	0.923077	0.135135	0.5
b_7	—	0.642857	—	—
b_8	—	0.5	—	—

TABLE IV. Parameters of the correlation in Eq. (19) for the expanded uncertainty of the third virial coefficient of ^4He and ^3He . T_0 is given in K, a in cm^6/mol^2 , b and c are dimensionless. For both isotopes, the correlations have been fitted with data in the range 2 – 3000 K and are therefore not reliable outside this range.

Parameter	^4He	^3He
T_0	100	100
a	6.506×10^{-3}	5.07×10^{-3}
b	1.59486	1.80741
c	0.422092	0.379443

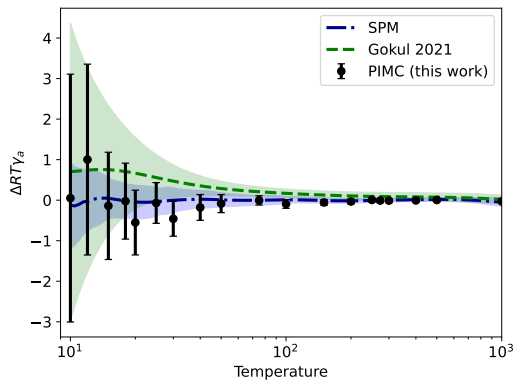


FIG. 8. Comparison of calculations of the third acoustic virial coefficient, $RT\gamma_a$, for ^4He . The baseline is the value obtained using the correlations of Eq. (18) for $B(T)$ and $C(T)$. The dot-dashed line reports the SPM evaluation of $RT\gamma_a$ obtained from the $C(T)$ curve computed in this work and the $B(T)$ data from Ref. 8. The blue shaded area reports the expanded uncertainty of $RT\gamma_a$ propagated using SPM. The black points are the path-integral results obtained in this work. The green curve reports the values obtained by Gokul *et al.*²⁹ together with their estimated expanded uncertainty.

3. Comparison with experiment

Extensive comparisons with experimental data for $C(T)$ and $RT\gamma_a(T)$ for ^4He were given in previous work.^{10,14} Already at that time, the uncertainties of calculated values were much smaller than those from experiment. We therefore limit our comparisons for $C(T)$ to cryogenic temperatures and to a few high-accuracy experimental sources near room temperature.

Figure 9 shows $C(T)$ near room temperature as points from Table II and as given by the fitting equation (18). Experimental values of C from three sources are plotted.^{30–32} For the datum of Gaiser and Fellmuth³² from dielectric-constant gas thermometry at 273.16 K, the quantity reported was a combination of density and dielectric virial coefficients; this was converted to C using the best calculated values for the second³³ and third³⁴ dielectric virial coefficients. Our results are consistent with these state-of-the-art experiments, but our uncertainties (which are much smaller than the size of the symbols) are smaller by at least two orders of magnitude.

Figure 10 shows a similar comparison for $C(T)$ below 40 K, where the available experimental sources^{35–40} are

TABLE V. Values of $RT\gamma_a$ for ^4He calculated in this work using PIMC or the SPM method, together with their expanded ($k = 2$) uncertainties. Temperatures are in units of K and $RT\gamma_a$ in units of cm^6/mol^2 .

T	$RT\gamma_a$ $U(RT\gamma_a)$		$RT\gamma_a$	$U(RT\gamma_a)$
	PIMC			
2	–	–	–29358	125
4	–	–	–5246	9
6	–	–	–680	4
8	–	–	457.6	1.9
10	806	3	806.1	1.1
12	906	2	905.2	0.7
15	900.6	1.3	900.8	0.5
18	841.5	0.9	841.5	0.4
20	794.7	0.8	795.2	0.4
25	684.5	0.5	684.54	0.34
30	591.0	0.4	591.42	0.30
40	453.6	0.3	453.76	0.22
50	360.2	0.2	360.25	0.18
75	224.07	0.11	224.07	0.12
100	151.96	0.11	152.06	0.09
150	78.95	0.07	78.99	0.06
200	43.10	0.06	43.12	0.06
250	22.40	0.05	22.38	0.05
273.16	15.58	0.05	15.59	0.05
300	9.17	0.05	9.18	0.04
400	–6.16	0.04	–6.14	0.04
500	–14.35	0.04	–14.33	0.04
1000	–26.10	0.03	–26.12	0.11
1500	–27.09	0.02	–	–
2000	–26.38	0.02	–	–

somewhat scattered. For clarity, we do not show error bars for the experimental sources; in some cases they were not reported, while in others they were on the order of several hundred $\text{cm}^6 \text{mol}^{-2}$. The uncertainty of our results is smaller than the size of the symbols; this can be compared with Fig. 2 of Ref. 10 where error bars for calculated results were visible below 5 K. Our results follow the general trend of the experimental data, but again have much smaller uncertainties.

The situation for the third acoustic virial coefficient is similar; agreement with available experimental data but with much smaller uncertainty. Figure 11 shows our calculations for ^4He compared to the values of $RT\gamma_a(T)$ derived in Ref. 10 from the sound-speed data of Gammon,⁴¹ along with a single value at 273.16 K reported by Gavioso *et al.*⁴² The agreement with experiment is good, but our uncertainties are smaller by at least one order of magnitude.

Figure 12 provides a similar comparison at temperatures below 20 K, where there are two experimental data sources.^{43,44} Again we use values of $RT\gamma_a(T)$ derived from these sound-speed data in Ref. 10. In this case, we have rescaled the ordinate for clarity and plotted the quantity $10^{-3}(T/1 \text{ K})RT\gamma_a$. Once again, our calculated results are consistent with experiment but have much smaller uncertainties.

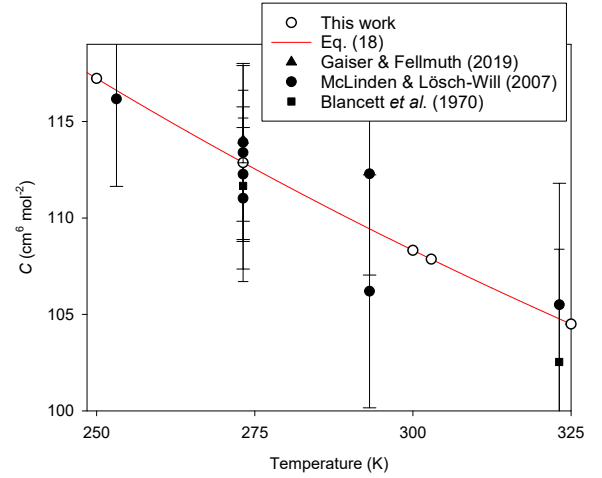


FIG. 9. Comparison of calculated $C(T)$ for ^4He with experimental values at near-ambient temperatures. Error bars on experimental points represent expanded uncertainties with coverage factor $k = 2$; expanded uncertainties for this work (see Table II) are much smaller than the symbols.

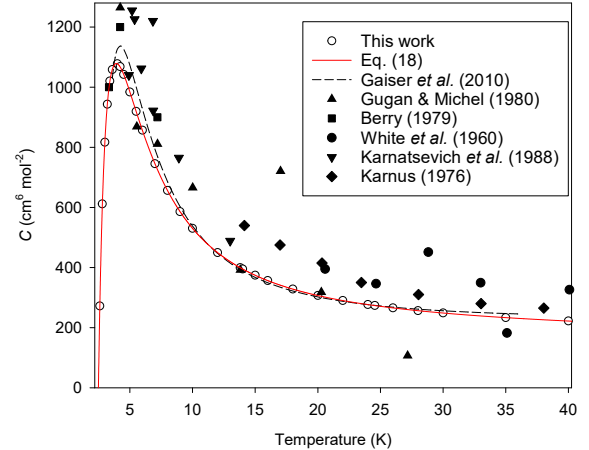


FIG. 10. Comparison of calculated $C(T)$ for ^4He with experimental values at low temperatures. Error bars on experimental points are not shown for clarity (see text); expanded uncertainties for this work (see Table II) are smaller than the symbols.

B. Helium-3

1. Third virial coefficient, $C(T)$

The situation for ^3He closely parallels that for ^4He . The improved pair and three-body potentials result in a roughly 5 times smaller uncertainty of $C(T)$ compared with our previously published results.¹⁰ The values of $C(T)$ computed in this work are reported in Tables VI and VII for the low and high temperature case, respectively. A graphical comparison with previous work is

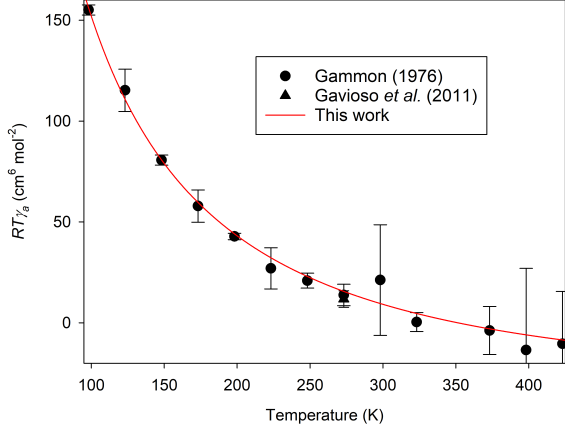


FIG. 11. Comparison of calculated $RT\gamma_a(T)$ for ^4He with experimental values. Error bars on experimental points represent expanded uncertainties with coverage factor $k = 2$; expanded uncertainties for this work (see Table V) are no larger than the width of the curve.

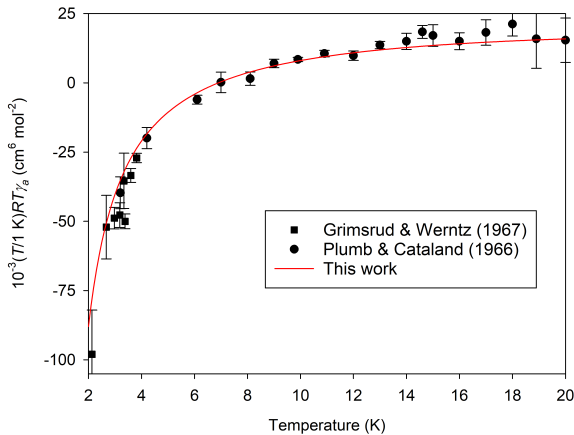


FIG. 12. Comparison of calculated $RT\gamma_a(T)$ for ^4He with experimental values at low temperatures. Error bars on experimental points represent expanded uncertainties with coverage factor $k = 2$; expanded uncertainties for this work (see Table V) are no larger than the width of the curve.

shown in Fig. 13, where one can see that our new values are in excellent agreement with the older results. Analogously to ^4He , we extended our calculations down to 0.5 K, rigorously including fermionic exchange effects.^{9,10}

2. Third acoustic virial coefficient, $RT\gamma_a$

To the best of our knowledge, no values of $RT\gamma_a$ for ^3He have appeared in the literature. We report our calculated values in Table VIII. Also in this case, we used SPM to propagate the uncertainty, as well as performing the calculation directly. In this case, the agreement between

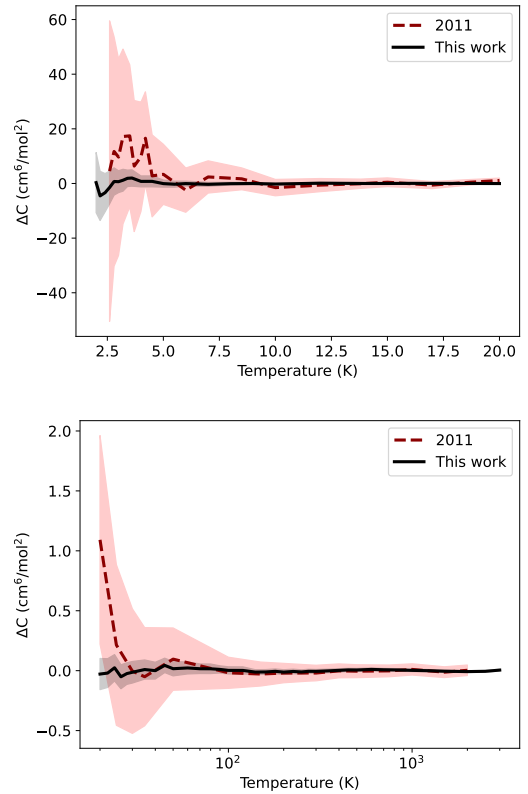


FIG. 13. Comparison between the values of $C(T)$ for ^3He calculated in this work (black solid line) and those available in the literature¹⁰ (red dashed line). We use as a baseline the correlation of Eq. (18). The shaded areas show the expanded ($k = 2$) uncertainty of the calculation that includes the statistical uncertainty and the uncertainty propagated from the pair and three-body potentials. Upper panel: lower temperatures. Lower panel: higher temperatures.

these two methods is very good, except at temperatures $T \gtrsim 500$ K for which, as already noted in Sec. III B, the SPM approach overestimates the uncertainty. Also for this isotope, SPM is the only way we can provide values of $RT\gamma_a$ and its uncertainty at temperatures where exchange effects are significant. For these reasons, we recommend the use of SPM-derived values of $RT\gamma_a$ and its uncertainty, which are reported as Supplementary Material.

V. CONCLUSIONS

Recent improvements in the pair potential⁸ and especially in the three-body potential¹³ for helium have allowed us to reduce the uncertainty of the third virial coefficient $C(T)$ calculated from first principles by approximately a factor of 4–5. These uncertainties are much smaller than those that can be obtained from even the best experiments; for example, the improvement over experiment is more than two orders of magnitude near 300

TABLE VI. The third virial coefficient $C(T)$ and its expanded ($k = 2$) uncertainty $U(C)$ for ^3He at low temperatures. The other columns report the contributions due to Boltzmann statistics (C_{Boltz}) and the odd (C_{odd}) and even exchange (C_{even}), together with their standard ($k = 1$) statistical uncertainties due to the Monte Carlo calculation. The last column reports the combined standard ($k = 1$) uncertainty propagated from the pair and three-body potentials. Temperatures are in units of K and $C(T)$ in units of cm^6/mol^2 .

T	C	$U(C)$	C_{Boltz}	$u(C_{\text{Boltz}})$	C_{odd}	$u(C_{\text{odd}})$	C_{even}	$u(C_{\text{even}})$	u_{pot}
0.5	-98152	2883	-71905	982	47368	912	-73614	451	282
0.6	-60497	1381	-38219	474	18060	452	-40338	155	157
0.8	-24901	512	-11514	206	1621	134	-15009	35	62
1	-11367	179	-3608	64	-1215	53	-6544	10	32
1.2	-4926	90	-329	32	-1430	25	-3166	7	19
1.4	-1694	51	1068	18	-1140	13	-1623	4	12
1.6	3	32	1673	11	-794	7	-875.7	1.8	8
1.8	840	22	1908	8	-576	4	-491.9	1.2	6
2	1285	11	1962	2	-394.9	1.7	-281.9	0.6	5
2.1768	1505	9	1968.6	1.7	-286.5	1.6	-177.5	0.4	4
2.4	1627	7	1914.5	1.3	-187.0	1.3	-100.8	0.3	3
2.6	1653	6	1846.9	1.1	-132.7	1.0	-61.51	0.18	3
2.8	1637	5	1768.2	0.9	-92.8	0.8	-38.63	0.10	2
3	1596	4	1688.0	0.8	-67.5	0.7	-24.59	0.07	1.8
3.2	1544	4	1607.8	0.7	-48.0	0.6	-15.91	0.05	1.5
3.4	1487	3	1531.0	0.7	-33.6	0.5	-10.33	0.03	1.3
3.6	1428	3	1459.0	0.6	-24.5	0.3	-6.81	0.02	1.2
4	1312	2	1329.1	0.5	-13.7	0.2	-3.083	0.010	0.9
4.5	1183.3	1.6	1190.8	0.4	-6.35	0.15	-1.190	0.006	0.7
5	1071.6	1.3	1075.1	0.3	-3.03	0.09	-0.488	0.002	0.6
5.5	977.7	1.1	979.5	0.3	-1.57	0.05	-0.204	0.001	0.5
6	898.6	0.9	899.3	0.2	-0.59	0.08	-0.090	0.001	0.4
7	773.2	0.7	773.45	0.16	-0.23	0.04	-0.019	0.000	0.3
8	680.7	0.5	680.76	0.12	-0.06	0.02	-0.004	0.000	0.2

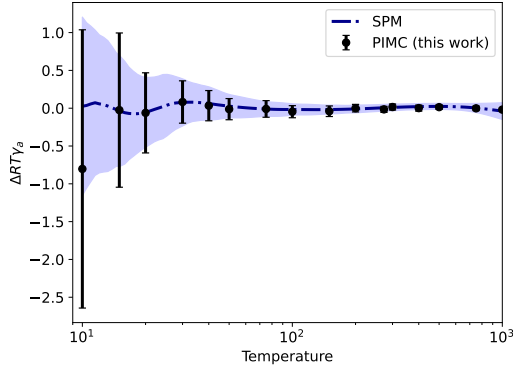


FIG. 14. Comparison of calculations of the third acoustic virial coefficient, $RT\gamma_a$, for ^3He . The baseline is the value obtained using the correlation of Eq. (18) for $B(T)$ and $C(T)$. The dot-dashed line reports the SPM evaluation of $RT\gamma_a$ obtained from the $C(T)$ curve computed in this work, and the $B(T)$ data from Ref. 8. The blue shaded area shows the expanded uncertainty of $RT\gamma_a$ propagated using SPM. The black points are the path-integral results obtained in this work.

K. It is clear that first-principles values have completely supplanted experiment for $C(T)$ of both ^4He and ^3He .

An improved propagator and other computational improvements for PIMC have allowed the temperature

range of first-principles $C(T)$ to be extended down to 0.5 K (compared to a previous lower limit of 2.6 K). To our knowledge, these are the first high-accuracy values of $C(T)$, either theoretical or experimental, to be obtained at such low temperatures.

For the third acoustic virial coefficient $\gamma_a(T)$, a new path-integral formula was employed that reduces the statistical uncertainty compared to the previous approach. However, even this improved approach produces undesirably large statistical uncertainties below about 50 K. In addition, exchange effects have not been implemented in the path-integral calculation of $\gamma_a(T)$, limiting its applicability to temperatures above approximately 6 K. Finally, because $\gamma_a(T)$ involves temperature derivatives of $C(T)$, it is not clear how to propagate the uncertainties of the potentials to an uncertainty in the acoustic virial coefficient.

We therefore implemented for the first time in such calculations the Schlessinger Point Method (SPM), a statistical approach that uses the $C(T)$ data and their uncertainties to obtain quantities involving derivatives and, most importantly, a reasonable estimate of the uncertainty of these quantities. The SPM is able to produce $\gamma_a(T)$ and its uncertainty throughout the range of $C(T)$ calculations.

There are several avenues for further reduction in the uncertainty, depending on the temperature range, as can be seen in the uncertainty budget shown in Fig. 1. At low

TABLE VII. The third virial coefficient $C(T)$ and its expanded ($k = 2$) uncertainty $U(C)$ for ^3He . The last two columns reports the standard ($k = 1$) statistical uncertainty due to the Monte Carlo calculation and the combined standard ($k = 1$) uncertainty propagated from the pair and three-body potentials. Temperatures are in units of K and $C(T)$ in units of cm^6/mol^2 .

T	C	$U(C)$	$u(C_{\text{Boltz}})$	u_{pot}
9	610.2	0.4	0.10	0.18
10	555.0	0.3	0.09	0.15
12	476.0	0.3	0.07	0.11
14	422.1	0.2	0.05	0.09
15	401.3	0.2	0.05	0.08
16	383.62	0.18	0.05	0.08
18	354.78	0.15	0.04	0.07
20	332.41	0.13	0.03	0.06
22	314.63	0.12	0.02	0.05
24	300.15	0.11	0.03	0.05
26	287.97	0.10	0.03	0.05
28	277.73	0.09	0.02	0.04
30	268.90	0.09	0.019	0.04
35	251.28	0.08	0.016	0.03
40	237.90	0.07	0.015	0.03
45	227.30	0.06	0.015	0.03
50	218.48	0.06	0.012	0.02
60	204.53	0.05	0.010	0.02
70	193.66	0.04	0.010	0.019
80	184.76	0.04	0.007	0.017
90	177.21	0.03	0.007	0.016
100	170.65	0.03	0.006	0.015
120	159.67	0.03	0.004	0.013
140	150.67	0.02	0.004	0.012
160	143.08	0.02	0.003	0.011
180	136.53	0.02	0.004	0.010
200	130.77	0.02	0.002	0.010
225	124.468	0.019	0.002	0.009
250	118.936	0.018	0.002	0.009
273.16	114.379	0.017	0.002	0.008
300	109.641	0.016	0.002	0.008
350	102.060	0.015	0.002	0.007
400	95.711	0.014	0.001	0.007
450	90.286	0.013	0.001	0.006
500	85.573	0.013	0.001	0.006
600	77.755	0.012	0.001	0.006
700	71.475	0.011	0.001	0.006
800	66.291	0.011	0.001	0.005
1000	58.160	0.010	0.001	0.005
1200	52.014	0.010	0.001	0.005
1500	45.091	0.009	0.001	0.004
2000	37.119	0.008	0.001	0.004
2500	31.646	0.008	0.001	0.004
3000	27.617	0.007	0.001	0.004

temperatures (below about 2 K), the largest contribution to our uncertainty budget is the statistical uncertainty in the PIMC calculations, which could be reduced at the expense of more computing time. At somewhat higher temperatures, up to about 10 K, the two-body potential is the largest source of uncertainty. Above 10 K, the largest uncertainty contribution comes from uncertainty in the three-body potential.

TABLE VIII. Values of $RT\gamma_a$ for ^3He calculated in this work using PIMC or the SPM method, together with their expanded ($k = 2$) uncertainties. Temperatures are in units of K and $RT\gamma_a$ in units of cm^6/mol^2 .

T	$RT\gamma_a$		$U(RT\gamma_a)$	
	PIMC	SPM	PIMC	SPM
2	–	–	–15379	143
4	–	–	–1427	29
6	–	–	564	4
8	–	–	1010.0	2.0
10	1091.79	1.84	1092.62	1.18
15	977.01	1.02	977.00	0.73
20	818.25	0.53	818.26	0.46
30	589.00	0.28	588.99	0.31
40	446.99	0.20	447.02	0.22
50	353.06	0.14	353.10	0.16
75	218.38	0.11	218.38	0.10
100	147.69	0.08	147.72	0.08
150	76.24	0.07	76.26	0.06
200	41.23	0.05	41.22	0.05
273.16	14.31	0.04	14.33	0.04
300	8.08	0.04	8.07	0.04
400	–6.91	0.04	–6.89	0.04
500	–14.89	0.03	–14.88	0.04
750	–23.50	0.03	–23.50	0.06
1000	–26.29	0.02	–26.31	0.11

Finally, we note that in some acoustic applications at higher pressures the fourth acoustic virial coefficient could be of interest. Direct PIMC calculation of this quantity would be quite difficult. However, the SPM method used here could be applied to the recent first-principles results for the fourth density virial coefficient $D(T)$ of helium⁴⁵ to provide the needed information for the fourth acoustic virial coefficient.

ACKNOWLEDGMENTS

G.G. acknowledges support from *Real-K* project 18SIB02, which has received funding from the EMPIR programme co-financed by the Participating States and from the European Union’s Horizon 2020 research and innovation programme. G.G. acknowledges CINECA (Award No. IskraC-RAVHE) under the ISCRA initiative for the availability of high-performance computing resources and support, and the University of Trento for a generous allocation of computing time.

Appendix A: Small variance estimation of acoustic virial coefficients

In the following derivations it will be convenient to evaluate derivatives with respect to the inverse temperature $\beta = (k_B T)^{-1}$, so that one has

$$T \frac{d}{dT} = -\beta \frac{d}{d\beta} \quad (\text{A1})$$

$$T^2 \frac{d^2}{dT^2} = 2\beta \frac{d}{d\beta} + \beta^2 \frac{d^2}{d\beta^2}. \quad (\text{A2})$$

1. Second acoustic virial

The second acoustic virial coefficient, $\beta_a(T)$, is defined as

$$\beta_a(T) = 2B(T) + 2(\gamma_0 - 1)T \frac{dB}{dT} + \frac{(\gamma_0 - 1)^2}{\gamma_0} T^2 \frac{d^2 B}{dT^2}, \quad (\text{A3})$$

where $B(T)$ is the density virial coefficient and in the case of a monoatomic system, $\gamma_0 = 5/3$.

In the path-integral approximation, the expression of the second virial coefficient $B(T)$ can be written as

$$B(T) = -\frac{N_A}{2} \int (e^{-\beta v(X)} - 1) F(X) dX \quad (\text{A4})$$

$$\equiv -\frac{N_A}{2} \int b(X) F(X) dX, \quad (\text{A5})$$

where X denotes the $6P - 3$ cartesian coordinates x_i ($i = 1, \dots, 6P - 3$) needed to describe a pair of ring polymers, $F(X)$ is the distribution function of ring polymer configurations and $v(X)$ is the pair potential averaged over the ring polymers.^{9,10,14} Equation (A5) is the definition of the quantity $b(X)$. The quantity $F(X)$ can be written as $Ae^{-\beta U}$, where U has the form of a harmonic potential and A is a (temperature dependent) proportionality constant. Given the expression of $F(X)$,^{9,10,14} it is straightforward to verify that

$$\frac{dF}{d\beta} = \left(U - \frac{3(P-1)}{2\beta} \right) F, \quad (\text{A6})$$

and hence

$$\frac{dB}{d\beta} = -\frac{N_A}{2} \int -v e^{-\beta v} F + (e^{-\beta v} - 1) \left(U - \frac{3(P-1)}{\beta} \right) F dX. \quad (\text{A7})$$

Notice that it is the presence of the terms coming from Eq. (A6) in Eq. (A7), which are similar to the *thermodynamic* estimator of the kinetic energy in the path-integral

approach,²³ that are responsible for the large statistical variance in our earlier calculation of acoustic virials.¹⁰

The fact that $U(X)$ has the form of a harmonic potential – *i.e.*, is a homogeneous function of degree two – enables the application of Euler's theorem which results in

$$2U = \sum_{i=1}^{6P-3} x_i \frac{\partial U}{\partial x_i}. \quad (\text{A8})$$

This result is at the heart of the derivation of the *virial* estimator of the kinetic energy.²⁴ In fact, one can write

$$\frac{\partial U}{\partial x_i} e^{-\beta U} = -\frac{1}{\beta} \frac{\partial}{\partial x_i} e^{-\beta U}, \quad (\text{A9})$$

and integrate by parts Eq. (A7) resulting in the expression

$$\frac{dB}{d\beta} = -\frac{N_A}{2} \int F \underbrace{\left[\frac{3}{2\beta} (e^{-\beta v} - 1) - W e^{-\beta v} \right]}_{\equiv Q} dX, \quad (\text{A10})$$

where

$$W = v + \sum_i \frac{x_i}{2} \frac{\partial v}{\partial x_i}. \quad (\text{A11})$$

At this point, we can evaluate the second derivative with respect to β of $B(T)$, obtaining

$$\frac{d^2 B}{d\beta^2} = -\frac{N_A}{2} \int \frac{dF}{d\beta} Q + F \left(W v e^{-\beta v} - \frac{3}{2\beta^2} (e^{-\beta v} - 1) - \frac{3v}{2\beta} e^{-\beta v} \right) dX. \quad (\text{A12})$$

In this case, the largest contribution to the variance comes from the first term, which we can again integrate by parts obtaining

$$\int \frac{dF}{d\beta} Q = \frac{1}{2\beta} \int F \left(3Q + \sum_i x_i \frac{\partial Q}{\partial x_i} \right) dX, \quad (\text{A13})$$

with

$$\frac{\partial W}{\partial x_i} = \frac{3}{2} \frac{\partial v}{\partial x_i} + \frac{1}{2} \sum_k x_k \frac{\partial^2 v}{\partial x_i \partial x_k} \quad (\text{A14})$$

$$\frac{\partial Q}{\partial x_i} = e^{-\beta v} \left[-\frac{\partial W}{\partial x_i} + \frac{\partial v}{\partial x_i} \left(\beta W - \frac{3}{2} \right) \right], \quad (\text{A15})$$

so that putting all together

$$\frac{d^2B}{d\beta^2} = -\frac{N_A}{2} \int \left[\frac{3\beta Q}{2} + \frac{1}{2} \sum_i x_i \frac{\partial \beta Q}{\partial x_i} + \left(\beta v \beta W - \frac{3\beta v}{2} \right) e^{-\beta v} - \frac{3}{2} (e^{-\beta v} - 1) \right] F \, dX \quad (\text{A16})$$

$$= -\frac{N_A}{2} \int \left[\frac{3}{4} (e^{-\beta v} - 1) + \beta v \beta W e^{-\beta v} + \frac{\beta e^{-\beta v}}{2} \left((\beta W - \frac{3}{2}) \mathbf{X} \cdot \nabla v - 6W - \frac{1}{2} \mathbf{X} \cdot \nabla^2 v \cdot \mathbf{X} \right) \right] F \, dX \quad (\text{A17})$$

$$\equiv -\frac{N_A}{2} \int S(X) \, dX, \quad (\text{A18})$$

where the last equation is the definition of $S(X)$.

Finally, we notice that due to translational and rotational invariance we can write

$$\mathbf{X} \cdot \nabla v = \sum_{i=1}^{6P-3} x_i \frac{\partial v}{\partial x_i} = \sum_{k=1}^P r^{(k)} \frac{\partial v}{\partial r^{(k)}} \quad (\text{A19})$$

$$\mathbf{X} \cdot \nabla^2 v \cdot \mathbf{X} = \sum_{ij} x_i x_j \frac{\partial^2 v}{\partial x_i \partial x_j} = \sum_{k=0}^P r^{(k)2} \frac{\partial^2 v}{\partial r^{(k)2}} \quad (\text{A20})$$

where $r^{(k)}$ is the distance between the two atoms in the imaginary-time slice k .

Equations (A3), (A10), and (A18) enable the evaluation of the second acoustic virial coefficient with a variance greatly reduced with respect to the straightforward application of temperature derivatives.

2. Third acoustic virial

The expression for the third acoustic virial coefficient is a bit more complicated²²

$$Q = B + (2\gamma_0 - 1)T \frac{dB}{dT} + (\gamma_0 - 1)T^2 \frac{d^2B}{dT^2} \quad (\text{A21})$$

$$RT\gamma_a = \left(\frac{\gamma_0 - 1}{\gamma_0} Q^2 - \beta_a(T)B(T) \right) + \frac{2\gamma_0 + 1}{\gamma_0} C + \frac{\gamma_0^2 - 1}{\gamma_0} T \frac{dC}{dT} + \frac{(\gamma_0 - 1)^2}{2\gamma_0} T^2 \frac{d^2C}{dT^2}, \quad (\text{A22})$$

but we can easily recognize a series of terms involving only two bodies (coming from Q , β_a , and the two-body part of $C(T)$) that can be evaluated using the approach outlined in the previous section.

a. The two-body contribution

We define the two-body contribution to $C(T)$ as

$$C_{2B}(T) = \int F(X)F(Y) (b(X) - 1) (b(Y) - 1) \, dX dY, \quad (\text{A23})$$

so that, from Eq. (A22), the two-body contribution to the third acoustic virial is then

$$RT\gamma_a^{(2B)} = \left(\frac{\gamma_0 - 1}{\gamma_0} Q^2 - \beta_a(T)B(T) \right) + \frac{2\gamma_0 + 1}{\gamma_0} C_{2B} + \frac{\gamma_0^2 - 1}{\gamma_0} T \frac{dC_{2B}}{dT} + \frac{(\gamma_0 - 1)^2}{2\gamma_0} T^2 \frac{d^2C_{2B}}{dT^2}, \quad (\text{A24})$$

which is most conveniently evaluated by defining

$$b_T(X) = -\beta Q(X) \quad (\text{A25})$$

$$b_{TT}(X) = \beta^2 S(X) - 2b_T(X). \quad (\text{A26})$$

After some lengthy but straightforward calculations, one ends up with

$$RT\gamma_a^{(2B)} = \int \left(\frac{2}{15} b_{TT}(X)b_{TT}(Y) + \frac{14}{15} b_T(X)b_{TT}(Y) + b(X)b_{TT}(Y) + \frac{73}{30} b_T(X)b_T(Y) + \frac{34}{5} b(X)b_T(Y) + \frac{33}{5} b(X)b(Y) \right) F(X)F(Y) \, dX dY. \quad (\text{A27})$$

b. The three-body contribution

Additionally, $RT\gamma_a(T)$ has a contribution from a purely three-body term, coming from the corresponding

contribution to $C(T)$

$$C_{3B}(T) = -\frac{1}{3} \int F(Z_3 - 3Z_2 + 2) \, dX, \quad (\text{A28})$$

that we are going to discuss in some detail, following the same steps of the previous section. The derivative with respect to β can be evaluated with the same integration-by-parts techniques outlined above, obtaining

$$\frac{\partial C_{3B}}{\partial \beta} = -\frac{1}{\beta} \int F(Z_3 - 3Z_2 + 2) dX + \frac{1}{3} \int F(W_3 Z_3 - 3W_2 Z_2) dX, \quad (\text{A29})$$

where we have used

$$\frac{\partial F}{\partial \beta} = F \left(U - \frac{9(P-1)}{2\beta} \right) \quad (\text{A30})$$

$$W_3 = V_3 + \frac{1}{2} \sum_{i=1}^{9(P-1)} x_i \frac{\partial V_3}{\partial x_i} \quad (\text{A31})$$

$$W_2 = V_2 + \frac{1}{2} \sum_i^{6(P-1)} x_i \frac{\partial V_2}{\partial x_i} \quad (\text{A32})$$

$$UF = -\frac{1}{2\beta} \sum_i x_i \frac{\partial F}{\partial x_i}, \quad (\text{A33})$$

where we have denoted by V_3 the total (additive + non-additive) three-body potential and by V_2 a two-body interaction. The second derivative with respect to β becomes:

$$\begin{aligned} \frac{\partial^2 C_{3B}}{\partial \beta^2} &= -\frac{2}{\beta^2} \int F(Z_3 - 3Z_2 + 2) dX + \\ &\frac{1}{3\beta} \int F \left[Z_3 W_3 \left(\frac{6}{\beta} - W_3 \right) - 3Z_2 W_2 \left(\frac{6}{\beta} - W_2 \right) \right] dX + \\ &\frac{1}{6\beta} \int F \left[Z_3 \left(\frac{1}{2} \mathbf{X} \cdot \nabla^2 V_3 \cdot \mathbf{X} + \frac{3}{2} \mathbf{X} \cdot \nabla V_3 \right) - \right. \\ &\left. 3Z_2 \left(\frac{1}{2} \mathbf{X} \cdot \nabla^2 V_2 \cdot \mathbf{X} + \frac{3}{2} \mathbf{X} \cdot \nabla V_2 \right) \right] dX. \end{aligned} \quad (\text{A34})$$

Using again translational and rotational invariance, and defining $R_1 = r_{12}$, $R_2 = r_{13}$ and $R_3 = r_{23}$, we can write

$$\mathbf{X} \cdot \nabla V_3 = \sum_{k=0}^P \sum_{i=0}^3 R_i^{(k)} \frac{\partial V_3}{\partial R_i^{(k)}}, \quad (\text{A35})$$

and

$$\mathbf{X} \cdot \nabla^2 V_3 \cdot \mathbf{X} = \sum_{k=0}^P \sum_{ij=0}^3 R_i^{(k)} R_j^{(k)} \frac{\partial^2 V_3}{\partial R_i^{(k)} \partial R_j^{(k)}}, \quad (\text{A36})$$

where the superscript (k) denotes an imaginary-time slice. Terms involving the derivatives of V_2 can be evaluated using Eqs. (A19) and (A20).

Appendix B: Statistical Schlessinger Point Method

1. The second acoustic virial coefficient for ^4He

Figure 15 reports the values of $B(T)$ reconstructed using the SPM approach, and compares them with the direct calculation obtained using the phase-shift approach.⁸

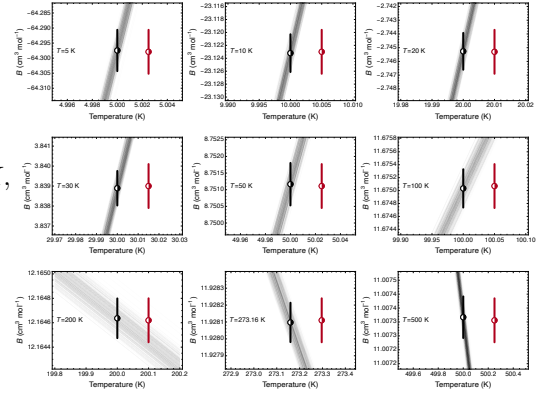


FIG. 15. Interpolating curves generated using the SPM method in the case of $B(T)$ for ^4He at various temperatures. The black symbol in each panel denotes the average value and $k = 2$ expanded uncertainty derived from the SPM curves. The red symbol, which has been displaced to the right for the sake of clarity, reports the average value and expanded uncertainty from the original calculation.⁸

Figure 16 reports the values of $\beta_a(T)$ reconstructed using the SPM approach, and compares them with the direct calculation obtained using the phase-shift approach.⁸

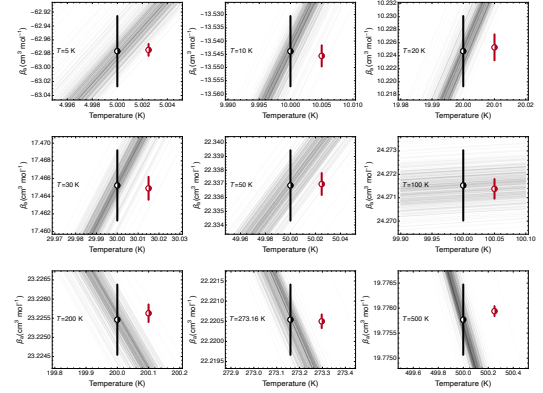


FIG. 16. Interpolating curves generated using the SPM method in the case of $\beta_a(T)$ for ^4He at various temperatures. The black symbol in each panel denotes the average value and $k = 2$ expanded uncertainty derived from the SPM curves. The red symbol, which has been displaced to the right for the sake of clarity, reports the average value and expanded uncertainty from the original calculation.⁸

2. The third acoustic virial coefficient for ^4He

Figure 17 reports the values of $C(T)$ reconstructed using the SPM approach, and compares them with the direct calculation obtained using the path-integral approach in this work.

Figure 18 reports the values of $RT\gamma_a(T)$ reconstructed using the SPM approach, and compares them with the

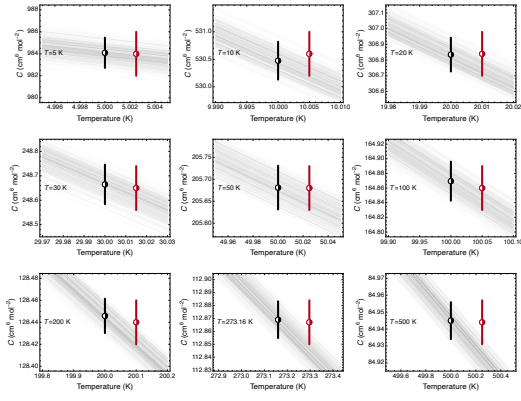


FIG. 17. Interpolating curves generated using the SPM method in the case of $C(T)$ for ${}^4\text{He}$ at various temperatures. The black symbol in each panel denotes the average value and $k = 2$ expanded uncertainty derived from the SPM curves. The red symbol, which has been displaced to the right for the sake of clarity, reports the average value and expanded uncertainty from path-integral Monte Carlo calculations performed in this work.

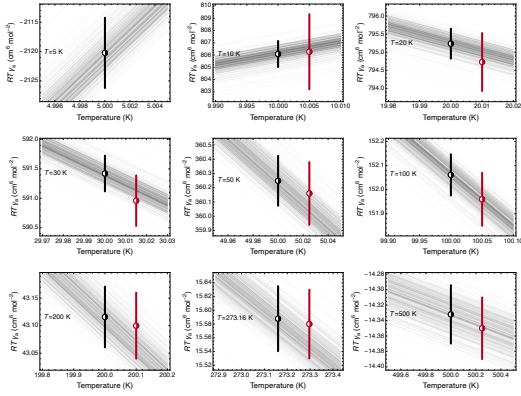


FIG. 18. Interpolating curves generated using the SPM method in the case of $RT\gamma_a(T)$ for ${}^4\text{He}$ at various temperatures. The black symbol in each panel denotes the average value and $k = 2$ expanded uncertainty derived from the SPM curves. The red symbol, which has been displaced to the right for the sake of clarity, reports the average value and expanded uncertainty from path-integral Monte Carlo calculations, which were performed in this work only for $T \geq 10$ K.

direct calculation obtained using path-integral approach in this work.

- ¹M. R. Moldover, R. M. Gavioso, J. B. Mehl, L. Pitre, M. de Podesta, and J. T. Zhang, “Acoustic gas thermometry,” *Metrologia* **51**, R1–R19 (2014).
- ²C. Gaiser, T. Zandt, and B. Fellmuth, “Dielectric-constant gas thermometry,” *Metrologia* **52**, S217–S226 (2015).
- ³P. M. C. Rourke, C. Gaiser, B. Gao, D. Madonna Ripa, M. R. Moldover, L. Pitre, and R. J. Underwood, “Refractive-index gas thermometry,” *Metrologia* **56**, 032001 (2019).
- ⁴P. M. C. Rourke, “Perspective on the refractive-index gas metrology data landscape,” *J. Phys. Chem. Ref. Data* **50**, 033104 (2021).
- ⁵C. Gaiser, B. Fellmuth, and W. Sabuga, “Primary gas-pressure standard from electrical measurements and thermophysical ab initio calculations,” *Nature Phys.* **16**, 177–180 (2020).
- ⁶C. Gaiser, B. Fellmuth, and W. Sabuga, “Primary gas pressure standard passes next stress test,” *Ann. Physik* **534**, 2200336 (2022).
- ⁷G. Garberoglio, C. Gaiser, R. Gavioso, A. H. Harvey, R. Hellmann, B. Jeziorski, K. Meier, M. R. Moldover, L. Pitre, K. Szalewicz, and R. Underwood, “Ab initio calculation of fluid properties for precision metrology,” *J. Phys. Chem. Ref. Data* **52**, 031502 (2023).
- ⁸P. Czachorowski, M. Przybytek, M. Lesiuk, M. Puchalski, and B. Jeziorski, “Second virial coefficients for ^4He and ^3He from an accurate relativistic interaction potential,” *Phys. Rev. A* **102**, 042810 (2020).
- ⁹G. Garberoglio and A. H. Harvey, “Path-integral calculation of the third virial coefficient of quantum gases at low temperatures,” *J. Chem. Phys.* **134**, 134106 (2011), Erratum: **152**, 199903 (2020).
- ¹⁰G. Garberoglio, M. R. Moldover, and A. H. Harvey, “Improved first-principles calculation of the third virial coefficient of helium,” *J. Res. Nat. Inst. Stand. Technol.* **116**, 729–742 (2011), Erratum: **125** 125019 (2020).
- ¹¹W. Cencek, M. Przybytek, J. Komasa, J. B. Mehl, B. Jeziorski, and K. Szalewicz, “Effects of adiabatic, relativistic, and quantum electrodynamics interactions on the pair potential and thermophysical properties of helium,” *J. Chem. Phys.* **136**, 224303 (2012).
- ¹²W. Cencek, K. Patkowski, and K. Szalewicz, “Full-configuration-interaction calculation of three-body nonadditive contribution to helium interaction potential,” *J. Chem. Phys.* **131**, 064105 (2009).
- ¹³J. Lang, G. Garberoglio, M. Przybytek, M. Jeziorska, and B. Jeziorski, “Three-body potential and third virial coefficients for helium including relativistic and nuclear-motion effects,” *Phys. Chem. Chem. Phys.* **25**, 23395 (2023).
- ¹⁴G. Garberoglio and A. H. Harvey, “First-principles calculation of the third virial coefficient of helium,” *J. Res. Nat. Inst. Stand. Technol.* **114**, 249–262 (2009).
- ¹⁵G. Garberoglio and A. H. Harvey, “Path-integral calculation of the fourth virial coefficient of helium isotopes,” *J. Chem. Phys.* **154**, 104107 (2021).
- ¹⁶R. P. Feynman and A. Hibbs, *Quantum Mechanics and Path Integrals* (McGraw-Hill, New York, 1965).
- ¹⁷M. Takahashi and M. Imada, “Monte Carlo calculation of quantum systems. II. Higher order correction,” *J. Phys. Soc. Jpn.* **53**, 3765 (1984).
- ¹⁸H. Kono, A. Takasak, and S. H. Lin, “Monte Carlo calculation of the quantum partition function via path integral formulations,” *J. Chem. Phys.* **88**, 6390 (1988).
- ¹⁹X.-P. Li and J. Broughton, “High-order correction to the Trotter expansion for use in computer simulation,” *J. Chem. Phys.* **86**, 5094 (1987).
- ²⁰K. R. S. Shaul, A. J. Schultz, and D. A. Kofke, “Path-integral Mayer-sampling calculations of the quantum Boltzmann contribution to virial coefficients of helium-4,” *J. Chem. Phys.* **137**, 184101 (2012).
- ²¹D. M. Ceperley, “Path integrals in the theory of condensed helium,” *Rev. Mod. Phys.* **67**, 279 (1995).
- ²²K. A. Gillis and M. R. Moldover, “Practical determination of gas densities from the speed of sound using square-well potentials,” *Int. J. Thermophys.* **17**, 1305–1324 (1996).
- ²³M. Tuckerman, *Statistical Mechanics: Theory and Molecular Simulation* (Oxford University Press, Oxford, UK, 2010).
- ²⁴M. F. Herman, E. J. Bruskin, and B. J. Berne, “On path integral Monte Carlo simulations,” *J. Chem. Phys.* **76**, 5150–5155 (1982).
- ²⁵L. Schlessinger, “Use of analyticity in the calculation of nonrelativistic scattering amplitudes,” *Phys. Rev.* **167**, 1411 (1968).
- ²⁶Sometimes this is also referred to as a multipoint-Padé expansion.
- ²⁷The SPM results have been proven to be independent of the number of input points, see *e.g.*, Ref. 46. Herein we always set $M = 20$ for the interpolation of both the second virial coefficient B (for which a total of $N = 122$ values were available) and the third one C (for which a smaller dataset of $N = 68$ values was available).
- ²⁸This is equivalent to requiring that statistical fluctuations in the replica subset do not cause the denominator Q_M^r appearing in Eq. (14) to develop real zeros on $\mathbb{R}_{>0}$.
- ²⁹N. Gokul, A. J. Schultz, and D. A. Kofke, “Speed of sound in helium-4 from ab initio acoustic virial coefficients,” *J. Chem. Eng. Data* **66**, 3258–3281 (2021).
- ³⁰A. L. Blancett, K. R. Hall, and F. B. Canfield, “Isotherms for the He–Ar system at 50°C, 0°C and –50°C up to 700 atm,” *Physica* **47**, 75–91 (1970).
- ³¹M. O. McLinden and C. Lössch-Will, “Apparatus for wide-ranging, high-accuracy fluid (p, ρ, T) measurements based on a compact two-sinker densimeter,” *J. Chem. Thermodyn.* **39**, 507–530 (2007).
- ³²C. Gaiser and B. Fellmuth, “Highly-accurate density-virial-coefficient values for helium, neon, and argon at 0.01 °C determined by dielectric-constant gas thermometry,” *J. Chem. Phys.* **150**, 134303 (2019).
- ³³G. Garberoglio and A. H. Harvey, “Path-integral calculation of the second dielectric and refractivity virial coefficients of helium, neon, and argon,” *J. Res. Natl. Inst. Stand. Technol.* **125**, 125022 (2020).
- ³⁴G. Garberoglio, A. H. Harvey, J. Lang, M. Przybytek, M. Lesiuk, and B. Jeziorski, “Path-integral calculation of the third dielectric virial coefficient of helium based on ab initio three-body polarizability and dipole surfaces,” In preparation (2024).
- ³⁵D. White, T. Rubin, P. Camky, and H. L. Johnston, “The virial coefficients of helium from 20 to 300°K,” *J. Phys. Chem.* **64**, 1607–1612 (1960).
- ³⁶A. I. Karnus, “Virial coefficients and some thermodynamic quantities of the helium isotopes in low temperature range,” *Ukr. Fiz. Zh.* **21**, 1179–1186 (1976).
- ³⁷K. H. Berry, “Measurements of the second and third virial coefficients of ^4He in the range 2.6–27.1 K,” *Mol. Phys.* **37**, 317–318 (1979).
- ³⁸D. Gugan and G. W. Michel, “Measurements of the polarizability and of the second and third virial coefficients of ^4He in the range 4.2–27.1 K,” *Mol. Phys.* **39**, 783–785 (1980).
- ³⁹L. V. Karnatsevich, I. V. Bogoyavlenskii, and L. P. Titov, “Virial coefficients of helium isotopes at low temperatures,” *Sov. J. Low Temp. Phys.* **14**, 1–7 (1988).
- ⁴⁰C. Gaiser, B. Fellmuth, and N. Haft, “Dielectric-constant gas-thermometry scale from 2.5 K to 36 K applying ^3He , ^4He , and neon in different temperature ranges,” *Int. J. Thermophys.* **31**, 1428–1437 (2010).
- ⁴¹B. E. Gammon, “The velocity of sound with derived state properties in helium at –175 to 150 °C with pressure to 150 atm,” *J. Chem. Phys.* **64**, 2556–2568 (1976).
- ⁴²R. M. Gavioso, G. Benedetto, D. Madonna Ripa, P. A. Giuliano Albo, C. Guianvarc’h, A. Merlone, L. Pitre, D. Truong, F. Moro, and R. Cuccaro, “Progress in INRiM experiment for the determination of the Boltzmann constant with a quasi-spherical resonator,” *Int. J. Thermophys.* **32**, 1339–1354 (2011).
- ⁴³D. T. Grimsrud and J. H. Werntz, “Measurements of the velocity of sound in He^3 and He^4 gas at low temperatures with implica-

- tions for the temperature scale,” *Phys. Rev.* **157**, 181–190 (1967).
- ⁴⁴H. Plumb and G. Cataland, “Acoustical thermometer and the National Bureau of Standards provisional temperature scale 2—20 (1965),” *Metrologia* **2**, 127–139 (1966).
- ⁴⁵R. J. Wheatley, G. Garberoglio, and A. H. Harvey, “Four-body nonadditive potential energy surface and the fourth virial coefficient of helium,” *J. Chem. Eng. Data* **68**, 3257–3264 (2023).
- ⁴⁶Z.-F. Cui, D. Binosi, C. D. Roberts, and S. M. Schmidt, “Fresh extraction of the proton charge radius from electron scattering,” *Phys. Rev. Lett.* **127**, 092001 (2021).